



OPEN ACCESS

EDITED BY

Wenbin Zheng,
Second Affiliated Hospital of Shantou
University Medical College, China

REVIEWED BY

Guanshu Liu,
Johns Hopkins University,
United States
Jianping Chu,
The First Affiliated Hospital, Sun
Yat-sen University, China

*CORRESPONDENCE

Weiwei Chen
✉ chenweiwei_tjh@tjh.tjmu.edu.cn

†These authors share first authorship

SPECIALTY SECTION

This article was submitted to
Neural Technology,
a section of the journal
Frontiers in Neuroscience

RECEIVED 22 November 2022

ACCEPTED 28 December 2022

PUBLISHED 11 January 2023

CITATION

Liao H, Cai Z, Ye H, Chen Q, Zhang Y,
Shaghghi M, Lutz SE, Chen W and
Cai K (2023) Combining *in vivo* proton
exchange rate (k_{ex}) MRI with
quantitative susceptibility mapping
to further stratify
the gadolinium-negative multiple
sclerosis lesions.
Front. Neurosci. 16:1105376.
doi: 10.3389/fnins.2022.1105376

COPYRIGHT

© 2023 Liao, Cai, Ye, Chen, Zhang,
Shaghghi, Lutz, Chen and Cai. This is
an open-access article distributed
under the terms of the [Creative
Commons Attribution License \(CC BY\)](#).
The use, distribution or reproduction in
other forums is permitted, provided
the original author(s) and the copyright
owner(s) are credited and that the
original publication in this journal is
cited, in accordance with accepted
academic practice. No use, distribution
or reproduction is permitted which
does not comply with these terms.

Combining *in vivo* proton exchange rate (k_{ex}) MRI with quantitative susceptibility mapping to further stratify the gadolinium-negative multiple sclerosis lesions

Huiting Liao^{1†}, Zimeng Cai^{2,3†}, Haiqi Ye^{1,4}, QianLan Chen^{1,5},
Yan Zhang¹, Mehran Shaghghi⁶, Sarah E. Lutz⁷,
Weiwei Chen^{1*} and Kejia Cai⁶

¹Department of Radiology, Tongji Hospital, Tongji Medical College, Huazhong University of Science and Technology, Wuhan, China, ²Department of Radiology, Guangdong Provincial People's Hospital, Guangdong Academy of Medical Sciences, Guangzhou, China, ³Guangdong Provincial Key Laboratory of Artificial Intelligence in Medical Image Analysis and Application, Guangdong Provincial People's Hospital, Guangdong Academy of Medical Sciences, Guangzhou, China, ⁴Department of Radiology, Hangzhou First People's Hospital, Zhejiang University School of Medicine, Hangzhou, China, ⁵Experimental and Clinical Research Center, Max Delbrück Center for Molecular Medicine and Charité – Universitätsmedizin Berlin, Corporate Member of Freie Universität Berlin, Berlin Institute of Health, Humboldt-Universität zu Berlin, Berlin, Germany, ⁶Department of Radiology, University of Illinois Hospital and Health Sciences System, Chicago, IL, United States, ⁷Department of Anatomy and Cell Biology, University of Illinois at Chicago College of Medicine, Chicago, IL, United States

Background: Conventional gadolinium (Gd)-enhanced MRI is currently used for stratifying the lesion activity of multiple sclerosis (MS) despite limited correlation with disability and disease activity. The stratification of MS lesion activity needs further improvement to better support clinics.

Purpose: To investigate if the novel proton exchange rate (k_{ex}) MRI combined with quantitative susceptibility mapping (QSM) may help to further stratify non-enhanced (Gd-negative) MS lesions.

Materials and methods: From December 2017 to December 2020, clinically diagnosed relapsing-remitting MS patients who underwent MRI were consecutively enrolled in this IRB-approved retrospective study. The customized MRI protocol covered conventional T₂-weighted, T₂-fluid-attenuated-inversion-recovery, pre- and post-contrast T₁-weighted imaging, and quantitative sequences, including k_{ex} MRI based on direct-saturation removed omega plots and QSM. Each MS lesion was evaluated based on its Gd-enhancement as well as its susceptibility and k_{ex} elevation compared to the normal appearing white matter. The difference and correlation concerning lesion characteristics and imaging contrasts were analyzed using the Mann–Whitney U test or Kruskal–Wallis test, and Spearman rank analysis with $p < 0.05$ considered significant.

Results: A total of 322 MS lesions from 30 patients were identified with 153 Gd-enhanced and 169 non-enhanced lesions. We found that the k_{ex} elevation of all lesions significantly correlated with their susceptibility elevation ($r = 0.30, p < 0.001$). Within the 153 MS lesions with Gd-enhancement, ring-enhanced lesions showed higher k_{ex} elevation than the nodular-enhanced ones' ($p < 0.001$). Similarly, lesions with ring-hyperintensity in QSM also had higher k_{ex} elevation than the lesions with nodular-QSM-hyperintensity ($p < 0.001$). Of the 169 Gd-negative lesions, three radiological patterns were recognized according to lesion manifestations on the k_{ex} map and QSM images: Pattern I (k_{ex}^+ and QSM⁺, $n = 114, 67.5\%$), Pattern II (only k_{ex}^+ or QSM⁺, $n = 47, 27.8\%$) and Pattern III (k_{ex}^- and QSM⁻, $n = 8, 4.7\%$). Compared to Pattern II and III, Pattern I had higher k_{ex} ($p < 0.001$) and susceptibility ($p < 0.05$) elevation. The percentage of Pattern I of each subject was negatively correlated with the disease duration ($r = -0.45, p = 0.015$).

Conclusion: As a potential imaging biomarker for inflammation due to oxidative stress, *in vivo* k_{ex} MRI combined with QSM is promising in extending the clinical classification of MS lesions beyond conventional Gd-enhanced MRI.

KEYWORDS

multiple sclerosis, magnetic resonance imaging, oxidative stress, iron, inflammation

Introduction

Multiple sclerosis (MS) is a chronic inflammatory demyelinating and neurodegenerative disorder of the central nervous system. Ongoing inflammation causes neuronal damage in MS patients (Kotelnikova et al., 2017). Clinical, radiological, and histological classification systems have been proposed (Pitt et al., 2022). Histological evidence of inflammation is incorporated to categorize lesions into early active, late active, smoldering, inactive, and shadow plaques (Frischer et al., 2015). Refinement of these classification systems to incorporate recently developed radiologic techniques for non-invasive evidence of inflammation may further guide clinical management and elucidation of disease pathogenesis.

To date, a commonly recognized classification in the clinic is to differentiate active (acute) from inactive lesions. Introducing gadolinium (Gd)-based contrast agents, Gd contrast-enhanced MRI can identify acute MS lesions (Tourdias et al., 2012), because the inflammatory infiltration led by lymphocytes and microglia can affect blood-brain-barrier (BBB) functions, allowing extravasation of gadolinium-based contrast agents (Lassmann et al., 2007). However, the gadolinium enhancement of acute lesions usually only lasts for weeks (Mahad et al., 2015). There is evidence suggesting that the gadolinium-enhanced lesions would turn into non-gadolinium-enhanced lesions even with inflammation continuously proceeding (Maggi et al., 2014). Moreover, the potential risk of Gd accumulation requires clinicians to make judicious use of this imaging method (Wattjes et al., 2021). Clinical practitioners may be able to make

more personalized treatments and monitor the therapeutic efficacy of treatment by reconsidering the interpretation of lesion activity, especially for Gd non-enhanced (Gd-negative) lesions.

There has been a significant amount of research dedicated to the recognition of smoldering lesions or detecting inflammatory changes in MS lesions. Quantitative susceptibility mapping (QSM) could reflect iron deposition when the relative lesion susceptibility value is above zero (Wisnieff et al., 2015). The susceptibility of MS lesions increases significantly when gadolinium-enhanced lesions evolve into non-gadolinium-enhanced lesions (Zhang et al., 2016b). In addition to iron, reactive oxygen species (ROS) are also reported to be key elements of inflammation (Dunham et al., 2017). The proton exchange rate (k_{ex}) MRI approach (Shaghghi et al., 2019), derived from chemical exchange saturation transfer (CEST) imaging, has recently been proposed as a non-invasive approach to assess tissue oxidative stress since endogenous ROS have been shown to promote *in vivo* k_{ex} in tissue (Tain et al., 2019; Shaghghi and Cai, 2022). Our team has previously conducted a preliminary study on k_{ex} MRI showing its potential to further characterize Gd-negative MS lesions (Ye et al., 2020). However, the contrast mechanism of k_{ex} -enhanced MRI as a surrogate biomarker for ROS has not been fully validated. Given that iron deposition catalyzes Fenton reaction that produces hydroxyl ROS (Tain et al., 2019), the correlation between QSM and k_{ex} MRI may help to validate k_{ex} MRI as an emerging inflammatory imaging contrast for MS stratification.

TABLE 1 Detailed parameters of each sequence.

Parameter	T1*	T2 [†]	T2 FLAIR [‡]	k_{ex} MRI [§]	ESWAN [¶]
Repetition time (msec)	500	5300	8400	3000	57
Effective echo time (msec)	8	92	145	22.6	4.3/4.8**
Slice thickness (mm)	5	5	5	5	2
Field of view (cm)	24	24	24	24	24
Matrix	320 × 320	512 × 512	512 × 512	128 × 128	512 × 512

*Pre- and post-contrast axial T₁-weighted fast spin-echo sequences (contrast agent: gadopentetate dimeglumine, Magnevist, Bayer, Berlin, Germany, 0.1 mmol/kg, IV).

[†] Axial T₂-weighted fast spin-echo sequences.

[‡] Axial T₂ fluid-attenuated inversion recovery sequences.

[§] Proton exchange rate MRI based on chemical exchange saturation transfer sequence.

[¶] Three-dimensional eight-echo T₂*-weighted angiography.

**First echo time/echo time spacing.

In the present study, we will compare k_{ex} MRI with the relatively well-established QSM in all MS lesions and investigate if the combination of k_{ex} MRI and QSM helps to stratify Gd-negative MS lesions based on lesion inflammatory activity.

Materials and methods

Participants

From December 2017 to December 2020, patients with relapsing-remitting MS in our institution who underwent MRI were consecutively included in the following institutional review board-approved retrospective study. All patients were clinically diagnosed according to the 2017 revision of the McDonald criteria (Thompson et al., 2018a). Cases with large motion artifacts were excluded. Relevant clinical information including major symptoms and Kurtzke Expanded Disability Status Scale (EDSS) scores was recorded. The onset date was also recorded according to the patients' questionnaire. The disease duration of each patient was estimated from the onset date to the day of receiving the MRI.

Image acquisition

All MRI exams were performed on a 3T GE MR750 unit (GE Healthcare, Milwaukee, WI) with a 32-channel head coil using a customized MRI protocol, including T₂-weighted imaging, T₂ fluid-attenuated inversion recovery (T₂-FLAIR) imaging, T₂*-weighted angiography for the QSM (Chen et al., 2014), CEST sequences for the k_{ex} MRI (Shaghaghi et al., 2019), and pre- and post-contrast T₁-weighted imaging. All sequences within the protocols were performed with matched slice positioning to allow lesion comparison between different MRI sequences. Post-contrast T₁-weighted imaging scans started 5 min after contrast agent administration (gadopentetate dimeglumine, Magnevist, Bayer, Berlin, Germany, 0.1 mmol/kg, IV).

The k_{ex} MRI protocol comprised three CEST Z-spectral data acquired with different saturation powers (B₁) at 2, 3, and 4 μT

and a saturation duration of 1.5 s, followed by a single-shot fast low angle shot readout. The total acquisition time of the three Z-spectra used for constructing omega plots was 9.9 min. At each saturation B₁, a total of 33 frequency offsets were obtained, including +39.1 ppm, +15.6 ppm, ±6 ppm, ±5 ppm, ±4.5 ppm, and frequencies ranging from -4 to +4 ppm with an increment of 0.25 ppm. CEST Z-spectral data were all acquired from a single slice covering most MS lesions as delineated by the T₂-FLAIR images. The target slice of each patient was decided by the same neuroradiologist (Q.C., 4 years of experience in neuroradiology). The detailed parameters of each sequence are summarized in Table 1.

Image reconstruction

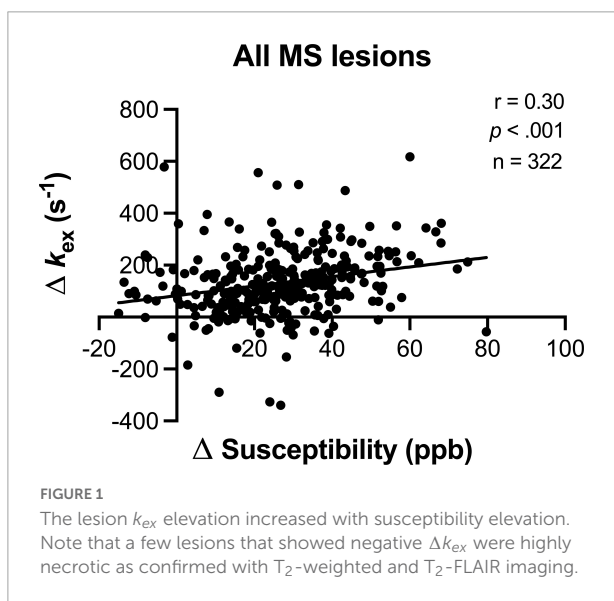
Quantitative susceptibility mapping was reconstructed based on the morphology enabled dipole inversion (MEDI) algorithm using in-house software implemented in C++ (Liu et al., 2012). The reconstruction was automatic without any user intervention. All acquired Z-spectral data were analyzed with the direct-saturation removed omega plot method (Shaghaghi et al., 2019) using MATLAB (MathWorks, Natick, MA, USA) with custom-written scripts. Equations were generated to reflect multiple exchange mechanisms, including NOE, MT, and CEST, that contribute to the saturation transfer signal (Shaghaghi et al., 2019). The reference image (39.1 ppm) from each CEST sequence was registered to that of B₁ = 3 μT sequence and each image within each CEST sequence was registered to its previous adjacent image. Z-spectra were normalized, flipped and fitted to two Lorentzian functions corresponding to the bulk water (centered around 0 ppm) and to a sum of the remaining effects (centered around 1.5 ppm). The frequency offset relative to water resonance, the center frequency offset, the amplitude, and the line-width of each peak were considered in the fitting function. After the fitting, the bulk water peak-the dominant component-was subtracted from the raw Z-spectra and the B₀-corrected residual signals at +3.5 ppm were used for further omega plot analysis. Tissue k_{ex} is a weighted average of multiple

exchange mechanisms. With the k_{ex} quantified for every voxel, k_{ex} maps were reconstructed.

Classification of MS lesions

Lesions with T2 hyperintensities (at least 3 mm on the long axis) were considered MS lesions in this study (Filippi et al., 2016). White matter regions without an abnormal signal were regarded as normal-appearing white matter (NAWM). Three neuroradiologists (H.L., Q.C., W.C., with 2, 4, and 20 years of experience in neuroradiology, respectively) independently reviewed all MRI images. The three observers assessed all MS lesions according to the presence of Gd enhancement, QSM hyperintensity, and k_{ex} elevation, as well as the lesion shape (nodular or ring) of Gd enhancement and QSM hyperintensity.

On post-contrast images, MS lesions were identified as enhanced (Gd-positive, Gd⁺) or non-enhanced (Gd-negative, Gd⁻). The Gd⁺ lesions were further classified as nodular-enhanced or ring-enhanced based on their shape. Lesions without QSM hyperintensity were considered QSM negative (QSM⁻), while lesions with QSM hyperintensity (QSM⁺) were also further categorized as nodular-QSM-hyperintense or ring-QSM-hyperintense (hyperintensity at the edge of the lesion). On the k_{ex} maps, we classified lesions into two groups: one without k_{ex} elevation (k_{ex}^-) and another with k_{ex} elevation (k_{ex}^+) relative to its adjacent or contralateral NAWM area. No further classification was performed based on the shape of the k_{ex}^+ lesion, as the k_{ex} elevation within each lesion was relatively uniform. Interobserver agreement for lesion classification was assessed and any difference was discussed, and a consensus was reached for further quantitative analyses.



Measurement of lesion k_{ex} elevation and susceptibility elevation

The k_{ex} elevation (Δk_{ex}) or susceptibility elevation ($\Delta \text{Susceptibility}$) of a lesion was defined as the difference of k_{ex} or susceptibility value between the lesion and its contralateral or adjacent NAWM area. The ROIs of k_{ex} and susceptibility were drawn using an in-house ROI tool of ITK-SNAP software (v4.0.0, Yushkevich et al., 2006) by two neuroradiologists (H.L. and Q.C.) independently. Taking T₂-FLAIR and T₂-weighted images as a reference, the lesion ROIs were drawn on the k_{ex} map and QSM images by hand, outlining the boundaries of each identified MS lesion. For inconspicuous lesions on the k_{ex} map or QSM images, the ROIs were first manually drawn on T₂-FLAIR images (or T₂-weighted images when they showed clear lesion boundaries) and then overlaid onto the k_{ex} map and QSM images. All veins or artifacts within lesions on QSM were also removed by hand. The ROIs of NAWM (rectangle, 4 mm²) were also placed on the mirror-symmetric area (or the adjacent NAWM of MS lesions if the mirror-symmetric area happened to be another lesion) as an internal reference. Interobserver agreement analysis was performed and the mean results of the two observers were used for further analyses.

Statistical analysis

Statistical analyses were performed by GraphPad Prism (v9.4.1) and SPSS (v26.0, IBM). Continuous variables were presented as mean \pm standard deviation, while categorical results were presented as fractions or percentages. Interobserver agreement between radiologists was measured by Fleiss' Kappa statistic (for the presence and shape of the lesion) or the intraclass correlation coefficient (for lesion measurement). The Kolmogorov–Smirnov test was used to determine the normality of the data. The comparison of lesion k_{ex} elevation or susceptibility elevation in subgroups was analyzed *via* the two-tailed Student's *t*-test and one-way ANOVA (Gaussian distribution) or Mann–Whitney U test and Kruskal–Wallis test (non-Gaussian distribution). The Spearman rank analysis were used to explore differences and correlations concerning lesion characteristics in different images. The statistical significance level, *p*, was set at 0.05.

Results

Demographic and clinical features

From December 2017 to December 2020, 34 patients with relapsing-remitting MS were identified and a total of 48 MRI exams were retrieved from the institutional database as 6 of

the 34 patients had one or more follow-up scans. Seven MRI exams from four patients were excluded for the failure of image reconstruction caused by motion artifacts. Ultimately, 30 patients and a total of 41 MRI examinations were included in the analysis, including data from five patients who had one or more follow-up exams. There were 21 women and 9 men. Their age ranged from 18 to 54 (mean \pm SD = 31.30 \pm 9.73) years old. The mean disease duration was 3.86 \pm 4.77 years (ranging from 0.05 to 20 years), with a median expanded disability status scale of 2.0 (ranging from 1.0 to 8.5). Demographic and clinical information with details are given in [Supplementary Table 1](#).

Lesion manifestation on QSM, k_{ex} , and post-contrast MRI

There was high agreement among observers in the assessment of the lesion presence, the lesion shape (Fleiss' Kappa coefficient $>$ 0.800 for both), and the quantitative measurement (intraclass correlation coefficient $>$ 0.800) ([Supplementary Table 2](#)). A total of 322 MS lesions were identified. The number of lesions with k_{ex} elevation ($n = 261$) or with QSM hyperintensity ($n = 282$) was larger than that with Gd-enhancement ($n = 153$). The k_{ex} elevation of MS lesions were positively and significantly correlated with the lesions' susceptibilities elevation ($r = 0.30$, $p < 0.001$, [Figure 1](#)). Note that a few lesions that showed negative Δk_{ex} in [Figure 1](#) were highly necrotic as confirmed with T₂-weighted and T₂-FLAIR imaging.

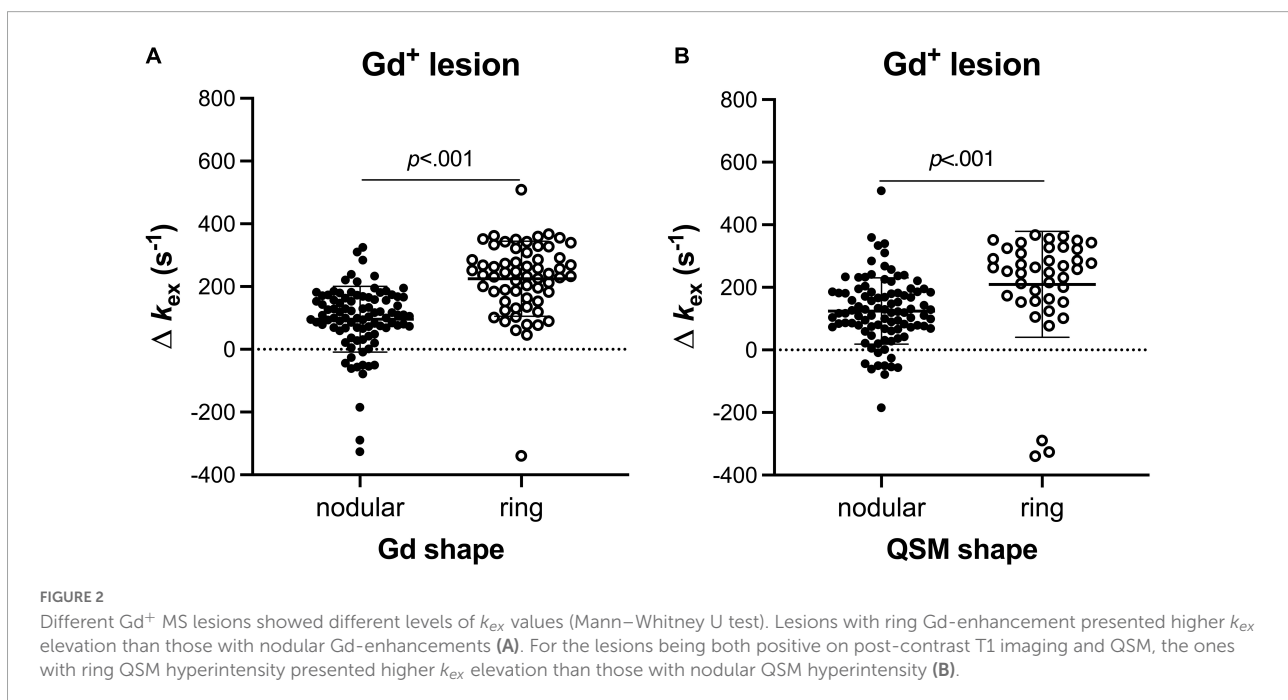
QSM and k_{ex} features in Gd⁺ lesions

In total, 153 MS lesions were Gd⁺. These Gd⁺ lesions showed two types of enhancement: ring-enhanced (61/153, 39.9%) and nodular-enhanced (92/153, 60.1%). The ring-enhanced ones presented higher k_{ex} elevation than the nodular-enhanced ones (225.0 \pm 119.2 s⁻¹ vs. 95.7 \pm 104.8 s⁻¹, $p < 0.001$, [Figure 2A](#)). On QSM, 89.5% (137/153) of the Gd⁺ lesions showed hyperintensity with two different shapes: nodular and ring-like. The lesions with ring-like QSM hyperintensity presented higher k_{ex} elevation than those with nodular QSM hyperintensity (209.7 \pm 169.6 s⁻¹ vs. 124.5 \pm 105.6 s⁻¹, $p < 0.001$, [Figure 2B](#)).

QSM and k_{ex} features in Gd⁻ MS lesions

52.5% (169/322) of MS lesions did not exhibit Gd enhancement. 76.9% (130/169) of Gd⁻ lesions showed k_{ex} elevation on the k_{ex} map and 85.7% (145/169) of Gd⁻ lesions showed hyperintensity on QSM. Of all Gd⁻ lesions, three radiological patterns covering four subtypes of MS lesions were recognized according to the lesion manifestation on the k_{ex} map and QSM images ([Figures 3, 4](#)).

Pattern I (k_{ex}^+ and QSM⁺, $n = 114$) took up the largest proportion of all Gd⁻ lesions, while Pattern III (k_{ex}^- and QSM⁻, $n = 8$) took up the smallest. Pattern II (only k_{ex}^+ or QSM⁺, $n = 47$) was composed of two subtypes: Pattern IIa (k_{ex}^+ and QSM⁻, $n = 16$) and Pattern IIb (k_{ex}^- and QSM⁺, $n = 31$).



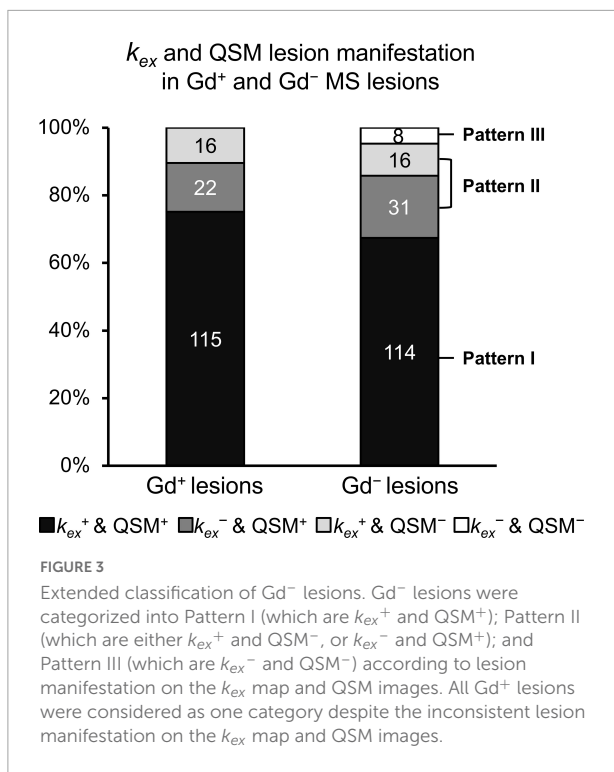


(Figure 3). The percentage of lesions of each pattern varied among cases (Figure 5). The percentage of Pattern I lesions in each patient was negatively correlated with disease duration ($r = -0.45$, $p = 0.015$, Figure 5A), while the percentage of Pattern II lesions was positively correlated with disease duration ($r = 0.38$, $p = 0.046$, Figure 5B).

Different levels of k_{ex} and susceptibility elevation were also observed within the three patterns (Figure 6). The Pattern I lesions presented higher k_{ex} and susceptibility elevation ($155.0 \pm 103.7 \text{ s}^{-1}$ and $28.19 \pm 12.87 \text{ ppb}$) than both Pattern II ($47.8 \pm 105.5 \text{ s}^{-1}$ and $20.16 \pm 14.67 \text{ ppb}$, $p < 0.001$) and Pattern III ($-19.61 \pm 45.74 \text{ s}^{-1}$ and $8.93 \pm 14.59 \text{ ppb}$, $p < 0.01$) lesions.

Discussion

In the present study, we further classified Gd⁻ lesions into three sub-patterns with different levels of k_{ex} and susceptibility elevation. Both k_{ex} and susceptibility elevation of Pattern I were higher than Pattern II. Furthermore, the patient with longer disease duration tended to have a lower percentage of lesions with Pattern I.

Multiple pathological processes occur during the course of MS, but the disruption of the BBB (Gaitan et al., 2011) the iron redistribution, and the oxidative damage (Dunham et al., 2017) are among the crucial inflammatory mechanisms. Assessing their correlation could be valuable for gaining a deeper understanding of lesion evolution.

In the present study, three MR imaging sequences (Gd-enhanced, QSM, and k_{ex} MRI) were used to compare the structural damage or the molecular changes from these three mechanisms, respectively. Gd enhancement usually suggests acute inflammation and consequential BBB disruption. The degree of axon demyelination and iron deposition could be reflected by susceptibility, while k_{ex} has been demonstrated to be able to reflect the overproduction of ROS due to oxidative stress (Tain et al., 2019).

On such premises, Patterns I & II could be regarded as radiologically active for at least one sequence suggesting the existence of inflammation, while Pattern III (which are Gd⁻, k_{ex}^- , and QSM⁻) might be considered radiologically inactive because inflammation was not detected by either QSM or k_{ex} MRI. Although the inconsistency of k_{ex} elevation and QSM hyperintensity did exist, over 70% of all MS lesions were consistently positive on both sequences, which is likely because iron can also serve as the catalyst for the Fenton reactions producing ROS (Tain et al., 2018). This finding suggests that the inflammation due to iron redistribution and oxygen burst can persist regardless of BBB repair. Therefore, interpreting all Gd⁻ lesions as inactive is inaccurate.

Ring enhancement, compared with nodular enhancement, has been considered to result in longer and more severe tissue damage (Davis et al., 2010). Patients with ring-enhancing lesions were also reported to be to reach a EDSS of 4.0–6.0 in shorter time (Llufriu et al., 2010). Ring hyperintensity on QSM, as a sign of iron-containing cells surrounding the lesion edge, has also been related to more severe demyelination and chronic lesion activity/expansion (Absinta et al., 2013; Zhang et al., 2016a). Of the Gd-enhanced lesions (the acute lesions), lesion k_{ex} elevation was higher in either ring Gd⁺ lesions or ring QSM⁺ lesions than in nodular lesions, which implies that k_{ex} elevation is positively correlated with the severity of lesion inflammation though further pathologic evidence based on animal experiments are pending for verification. Endogenous ROS of MS is reported to come from the oxygen burst in microglia, inducing mitochondrial dysfunction and subsequent histotoxic hypoxia (Fischer et al., 2012). This further results in energy deficiency and ionic imbalance in oligodendrocytes, axons, and neurons (Mahad et al., 2015). When the respiratory burst leads to cellular degradation, the ferrous iron released from microglia and macrophages may in turn amplify inflammatory oxidative injury and neurodegeneration (Haider, 2015). The mild positive correlation between susceptibility and k_{ex} elevation we found may just reflect the interplay of iron content and ROS in MS lesions.

Based on the potential mutual reinforcement of iron deposition and oxygen damage, Pattern I is more likely to be inflammatory than Pattern II. For patients with relapsing-remitting courses, the inflammatory status of lesions might not always stay at the same level; instead, it could drop

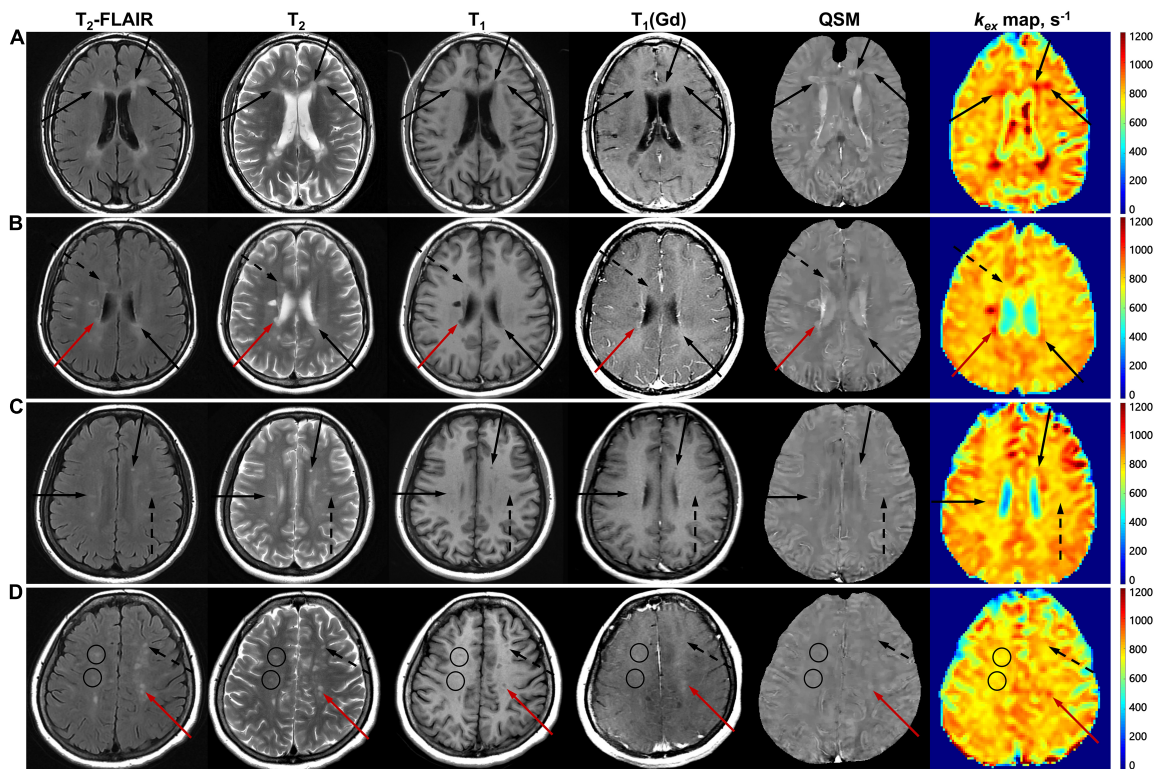


FIGURE 4
 Gd⁺ lesions and the three patterns of Gd⁻ lesions on multimodal MRI. Images are from Patient No. 20 (A), No. 13 (B), No. 11 (C), and No. 27 (D), whose disease duration was 0.5, 1, 2, and 8 years, respectively. Gd⁺ lesions are indicated with red arrows (B,D). Pattern I of Gd⁻ lesions, which are k_{ex}^+ and QSM⁺, are indicated with black arrows (A–C). Pattern II of Gd⁻ lesions, which are either k_{ex}^+ and QSM⁻, or k_{ex}^- and QSM⁺, are indicated with black dashed arrows (B–D). Pattern III of Gd⁻ lesions, which are k_{ex}^- and QSM⁻, are indicated with black circles (D).

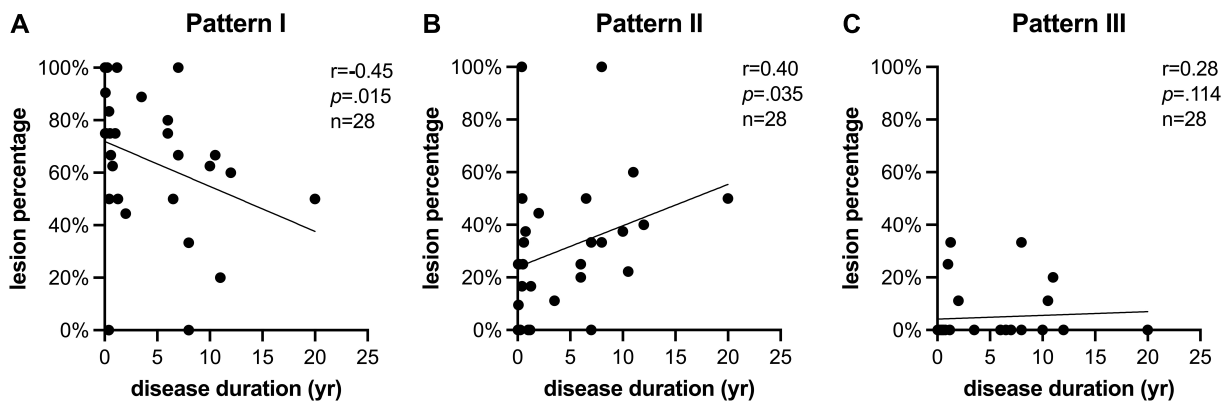
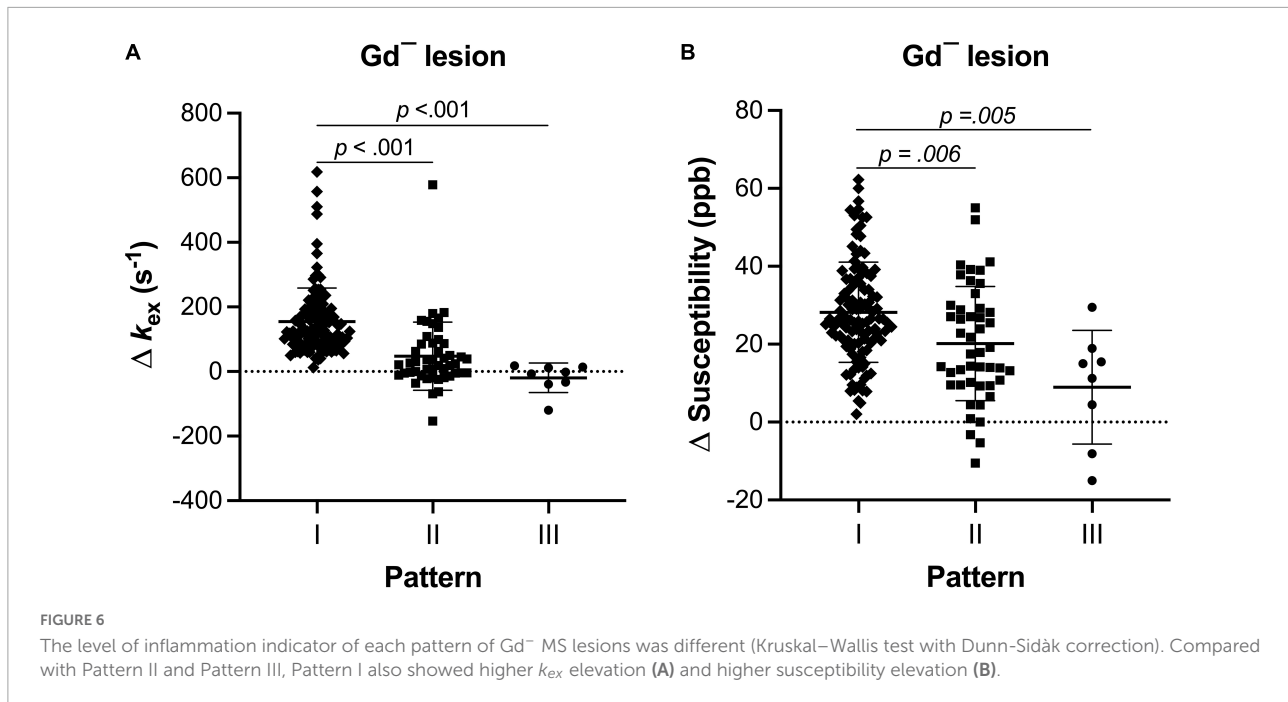


FIGURE 5
 k_{ex} multimodal MRI pattern is related to disease duration. The percentage of lesions identified as (A) Pattern I (which are k_{ex}^+ and QSM⁺); (B) Pattern II (which are either k_{ex}^+ and QSM⁻, or k_{ex}^- and QSM⁺); and (C) Pattern III (which are k_{ex}^- and QSM⁻) changed with the disease duration of the case. Cases with long disease duration showed smaller percentage of Pattern I but larger percentage of Pattern II in Gd⁻ lesions than cases with short disease duration.

from a higher level to a lower one. The change in the percentage of Pattern I lesions with disease duration might reflect such evolution of chronic inflammation. As for the change in the percentage of Pattern II lesions, it may

represent the combination of two different evolutionary trends, since Pattern II consists of two subtypes: IIa (which are k_{ex}^+ and QSM⁻) and IIb (which are k_{ex}^- and QSM⁺). Comparing to the other two patterns, a relatively larger



standard deviation of k_{ex} elevation in Pattern II might also reflect the highly heterogenous nature of it. In the present study, the two subtypes were integrated into one pattern because of the possibly similar level of inflammation, which was lower than Pattern I but higher than Pattern III. The difference between k_{ex} MRI and QSM reflects their differences in contrast mechanism. Nevertheless, attributing k_{ex} MRI contrast to oxidative stress and ROS production and comparing iron-induced inflammation requires further validation with biochemical analyses.

Lesion susceptibility elevation has generally been reported to remain relatively stable for months or years (Stuber et al., 2016), but lesion k_{ex} elevation may possess a more volatile trait since if the balance of pro- and antioxidants has not been achieved, ROS may not cease to fluctuate. Unlike the other two imaging sequences, the more susceptible ROS production seems to make the k_{ex} map a more sensitive method for inflammation indication and curative response monitoring. By enhancing the sensitivity and specificity, the combination of k_{ex} and QSM MRI could help to further stratify the lesion inflammatory status and detect smoldering lesions after the acute stage. In combination with QSM, k_{ex} MRI is promising for detection of lesion inflammation or activity.

Clinically, MS patients with a slow or moderate disease course typically receive a moderately effective and very safe medication, whereas patients who demonstrate highly active or rapidly evolving disease are candidates for highly effective but potentially less safe treatment (Thompson et al., 2018b). The time lost in the wait-and-see approach delays highly critical intervention for patients who are later identified as rapidly

progressing. Therefore, an improved ability to risk-stratify MS lesion activity with k_{ex} MRI would help predict prognosis and guide treatment. The clinicians might also utilize non-invasive longitudinal k_{ex} MRI to monitor the therapeutic efficacy of treatment. For example, a drop of Pattern I percentage in all MS lesions might suggest good treatment response. With an extended lesion classification, a more personalized treatment is facilitated.

This study presents a preliminary exploration of the feasibility of QSM and k_{ex} MRI in MS lesion categorization based on retrospective, cross-sectional, single-center data. The sample size is relatively small, and the small lesion amount affected the statistical analysis of the two subtypes of Pattern II as well as Pattern III. To conform with k_{ex} MRI, the image analysis was limited to one slice of image for each case and was also restricted by the spatial resolution of Z-spectral MRI. The errors on lesion registration and k_{ex} measurement may exist because there are small lesions which are challenging to differentiate from potential ischemic lesions. Moreover, further validation with pathological studies on preclinical animal models is needed. Research with larger samples, prospective and longitudinal designs, and invasive biochemical validation should be carried out.

In conclusion, the study extended the classification of MS lesions by the combination of three MRI sequences (Gd-enhanced, QSM, and k_{ex} MRI). Underlying inflammation of Gd⁻ lesions was further visualized by QSM and k_{ex} MRI, suggesting their utility in assessing the inflammation status of lesions previously considered inactive with Gd-enhanced MRI.

Data availability statement

The raw data supporting the conclusions of this article will be made available by the authors, without undue reservation.

Ethics statement

The studies involving human participants were reviewed and approved by the Institutional Review Board of Tongji Hospital, Tongji Medical College, Huazhong University of Science and Technology. Written informed consent for participation was not required for this study in accordance with the national legislation and the institutional requirements.

Author contributions

HL: analysis and interpretation of data, drafting and revision of the manuscript for content, including medical writing for content, and study concept or design. ZC: processing, analysis and interpretation of data, drafting of the manuscript for content, and including medical writing for content. HY and QC: major role in the acquisition of data and analysis of data. YZ: acquisition of data. MS and SL: revision of the manuscript for content and including medical writing for content. WC: study concept or design, acquisition and interpretation of data, and revision of the manuscript for content. KC: study concept or design, interpretation of data, and revision of the manuscript for content. All authors contributed to the article and approved the submitted version.

References

- Absinta, M., Sati, P., Gaitan, M. I., Maggi, P., Cortese, I. C., Filippi, M., et al. (2013). Seven-tesla phase imaging of acute multiple sclerosis lesions: A new window into the inflammatory process. *Ann. Neurol.* 74, 669–678. doi: 10.1002/ana.23959
- Chen, W., Gauthier, S. A., Gupta, A., Comunale, J., Liu, T., Wang, S., et al. (2014). Quantitative susceptibility mapping of multiple sclerosis lesions at various ages. *Radiology* 271, 183–192. doi: 10.1148/radiol.13130353
- Davis, M., Auh, S., Riva, M., Richert, N. D., Frank, J. A., McFarland, H. F., et al. (2010). Ring and nodular multiple sclerosis lesions: A retrospective natural history study. *Neurology* 74, 851–856. doi: 10.1212/WNL.0b013e3181d31df5
- Dunham, J., Bauer, J., Campbell, G. R., Mahad, D. J., van Driel, N., van der Pol, S. M. A., et al. (2017). Oxidative injury and iron redistribution are pathological hallmarks of marmoset experimental autoimmune encephalomyelitis. *J. Neuropathol. Exp. Neurol.* 76, 467–478. doi: 10.1093/jnen/nlx034
- Filippi, M., Rocca, M. A., Ciccarelli, O., De Stefano, N., Evangelou, N., Kappos, L., et al. (2016). MRI criteria for the diagnosis of multiple sclerosis: MAGNIMS consensus guidelines. *Lancet Neurol.* 15, 292–303. doi: 10.1016/s1474-4422(15)00393-2
- Fischer, M. T., Sharma, R., Lim, J. L., Haider, L., Frischer, J. M., Drexhage, J., et al. (2012). NADPH oxidase expression in active multiple sclerosis lesions in relation to oxidative tissue damage and mitochondrial injury. *Brain* 135(Pt 3), 886–899. doi: 10.1093/brain/awo012
- Frischer, J. M., Weigand, S. D., Guo, Y., Kale, N., Parisi, J. E., Pirko, I., et al. (2015). Clinical and pathological insights into the dynamic nature of the white matter multiple sclerosis plaque. *Ann. Neurol.* 78, 710–721. doi: 10.1002/ana.24497
- Gaitan, M. I., Shea, C. D., Evangelou, I. E., Stone, R. D., Fenton, K. M., Bielekova, B., et al. (2011). Evolution of the blood-brain barrier in newly forming multiple sclerosis lesions. *Ann. Neurol.* 70, 22–29. doi: 10.1002/ana.22472
- Haider, L. (2015). Inflammation, iron, energy failure, and oxidative stress in the pathogenesis of multiple sclerosis. *Oxid. Med. Cell. Longev.* 2015:725370. doi: 10.1155/2015/725370
- Kotelnikova, E., Kiani, N. A., Abad, E., Martinez-Lapiscina, E. H., Andorra, M., Zubizarreta, I., et al. (2017). Dynamics and heterogeneity of brain damage in multiple sclerosis. *PLoS Comput. Biol.* 13:e1005757. doi: 10.1371/journal.pcbi.1005757
- Lassmann, H., Bruck, W., and Lucchinetti, C. F. (2007). The immunopathology of multiple sclerosis: An overview. *Brain Pathol.* 17, 210–218. doi: 10.1111/j.1750-3639.2007.00064.x
- Liu, T., Xu, W., Spincemaille, P., Avestimehr, A. S., and Wang, Y. (2012). Accuracy of the morphology enabled dipole inversion (MEDI) algorithm for quantitative susceptibility mapping in MRI. *IEEE Trans. Med. Imaging* 31, 816–824. doi: 10.1109/TMI.2011.2182523
- Llufriu, S., Pujol, T., Blanco, Y., Hankiewicz, K., Squarcia, M., Berenguer, J., et al. (2010). T2 hypointense rims and ring-enhancing lesions in MS. *Mult. Scler.* 16, 1317–1325. doi: 10.1177/1352458510377905

Acknowledgments

We wish to thank Dr. Bruce Ozgen Mocan for her advice on the manuscript and figure preparation.

Conflict of interest

The authors declare that the research was conducted in the absence of any commercial or financial relationships that could be construed as a potential conflict of interest.

Publisher's note

All claims expressed in this article are solely those of the authors and do not necessarily represent those of their affiliated organizations, or those of the publisher, the editors and the reviewers. Any product that may be evaluated in this article, or claim that may be made by its manufacturer, is not guaranteed or endorsed by the publisher.

Supplementary material

The Supplementary Material for this article can be found online at: <https://www.frontiersin.org/articles/10.3389/fnins.2022.1105376/full#supplementary-material>

- Maggi, P., Macri, S. M., Gaitan, M. I., Leibovitch, E., Wholer, J. E., Knight, H. L., et al. (2014). The formation of inflammatory demyelinated lesions in cerebral white matter. *Ann. Neurol.* 76, 594–608. doi: 10.1002/ana.24242
- Mahad, D. H., Trapp, B. D., and Lassmann, H. (2015). Pathological mechanisms in progressive multiple sclerosis. *Lancet Neurol.* 14, 183–193. doi: 10.1016/s1474-4422(14)70256-x
- Pitt, D., Lo, C. H., Gauthier, S. A., Hickman, R. A., Longbrake, E., Airas, L. M., et al. (2022). Toward precision phenotyping of multiple sclerosis. *Neurol. Neuroimmunol. Neuroinflamm.* 9:e200025. doi: 10.1212/NXI.0000000000200025
- Shaghghi, M., and Cai, K. (2022). Toward in vivo MRI of the tissue proton exchange rate in humans. *Biosensors (Basel)* 12:815. doi: 10.3390/bios12100815
- Shaghghi, M., Chen, W., Scotti, A., Ye, H., Zhang, Y., Zhu, W., et al. (2019). In vivo quantification of proton exchange rate in healthy human brains with omega plot. *Quant. Imaging Med. Surg.* 9, 1686–1696. doi: 10.21037/qims.2019.08.06
- Stuber, C., Pitt, D., and Wang, Y. (2016). Iron in multiple sclerosis and its noninvasive imaging with quantitative susceptibility mapping. *Int. J. Mol. Sci.* 17:100. doi: 10.3390/ijms17010100
- Tain, R. W., Scotti, A. M., and Cai, K. (2019). Improving the detection specificity of endogenous MRI for reactive oxygen species (ROS). *J. Magn. Reson. Imaging* 50, 583–591. doi: 10.1002/jmri.26629
- Tain, R. W., Scotti, A. M., Li, W., Zhou, X. J., and Cai, K. (2018). Imaging short-lived reactive oxygen species (ROS) with endogenous contrast MRI. *J. Magn. Reson. Imaging* 47, 222–229. doi: 10.1002/jmri.25763
- Thompson, A. J., Banwell, B. L., Barkhof, F., Carroll, W. M., Coetzee, T., Comi, G., et al. (2018a). Diagnosis of multiple sclerosis: 2017 revisions of the McDonald criteria. *Lancet Neurol.* 17, 162–173. doi: 10.1016/s1474-4422(17)30470-2
- Thompson, A. J., Baranzini, S. E., Geurts, J., Hemmer, B., and Ciccarelli, O. (2018b). Multiple sclerosis. *Lancet* 391, 1622–1636. doi: 10.1016/S0140-6736(18)30481-1
- Tourdias, T., Roggerone, S., Filippi, M., Kanagaki, M., Rovaris, M., Miller, D. H., et al. (2012). Assessment of disease activity in multiple sclerosis phenotypes with combined gadolinium- and superparamagnetic iron oxide-enhanced MR imaging. *Radiology* 264, 225–233. doi: 10.1148/radiol.12111416
- Wattjes, M. P., Ciccarelli, O., Reich, D. S., Banwell, B., de Stefano, N., Enzinger, C., et al. (2021). 2021 MAGNIMS–CMSC–NAIMS consensus recommendations on the use of MRI in patients with multiple sclerosis. *Lancet Neurol.* 20, 653–670. doi: 10.1016/s1474-4422(21)00095-8
- Wisnieff, C., Ramanan, S., Olesik, J., Gauthier, S., Wang, Y., and Pitt, D. (2015). Quantitative susceptibility mapping (QSM) of white matter multiple sclerosis lesions: Interpreting positive susceptibility and the presence of iron. *Magn. Reson. Med.* 74, 564–570. doi: 10.1002/mrm.25420
- Ye, H., Shaghghi, M., Chen, Q., Zhang, Y., Lutz, S. E., Chen, W., et al. (2020). In vivo proton exchange rate (kex) MRI for the characterization of multiple sclerosis lesions in patients. *J. Magn. Reson. Imaging* 53, 408–415. doi: 10.1002/jmri.27363
- Yushkevich, P. A., Piven, J., Hazlett, H. C., Smith, R. G., Ho, S., Gee, J. C., et al. (2006). User-guided 3D active contour segmentation of anatomical structures: Significantly improved efficiency and reliability. *Neuroimage* 1, 1116–1128. doi: 10.1016/j.neuroimage.2006.01.015
- Zhang, Y., Gauthier, S. A., Gupta, A., Comunale, J., Chia-Yi Chiang, G., Zhou, D., et al. (2016b). Longitudinal change in magnetic susceptibility of new enhanced multiple sclerosis (MS) lesions measured on serial quantitative susceptibility mapping (QSM). *J. Magn. Reson. Imaging* 44, 426–432. doi: 10.1002/jmri.25144
- Zhang, Y., Gauthier, S. A., Gupta, A., Chen, W., Comunale, J., Chiang, G. C., et al. (2016a). Quantitative susceptibility mapping and R2* measured changes during white matter lesion development in multiple sclerosis: Myelin breakdown, myelin debris degradation and removal, and iron accumulation. *AJNR Am. J. Neuroradiol.* 37, 1629–1635. doi: 10.3174/ajnr.A4825